Femtosecond Time-Resolved Dynamics of Geminate and Nongeminate Recombination: Iodine Enclosed in the Nanocavities of a Microporous SiO_2 Modification†

G. Flachenecker,‡ P. Behrens,§ G. Knopp,‡ M. Schmitt,‡ T. Siebert,‡ A. Vierheilig,‡ G. Wirnsberger,|| and A. Materny*,‡

Institut für Physikalische Chemie der Universität Würzburg, Am Hubland, D-97074 Würzburg, Germany, Institut für Anorganische Chemie der Universität Hannover, Callinstr. 9, D-30167 Hannover, Germany, Institut für Anorganische Chemie der Karl−Franzens−Universität Graz, Schubertstr. 1, A-8010 Graz, Austria

Received: January 7, 1999; In Final Form: March 9, 1999

In this study, we report the ultrafast dissociation and recombination dynamics of I_2 enclosed in well-defined cages formed by the electroneutral host framework of the crystalline microporous SiO_2 modification decadodecasil 3R (DDR). In this composite, each cage is occupied by one guest molecule, corresponding to a high density of I_2. The dynamics are investigated by femtosecond pump−probe spectroscopy with variable probe wavelengths. After excitation into the bound B state, collision-induced predissociation is observed followed by recombination onto the A and A′ states, where the molecules undergo vibrational relaxation. A kinetic model is applied to simulate the experimental data. The results are compared with results from a former study [Materny et al. *J. Phys. Chem.* **1996**, *100*, 18650] where I_2 predissociation and caging dynamics in compressed argon were probed along the reaction coordinate. Geminate primary recombination (within the cage) is characterized by rate constants which are nearly identical to those found for I_2 in Ar at 200−400 bar. No geminate secondary recombination (diffusive, outside the cage) is observed. However, approximately 10% of the recombinations are assumed to be nongeminate with a rate that corresponds to the motion of iodine atoms into the adjacent cages.

1. Introduction

Since Franck and Rabinowitch[1−3] first proposed that solvents can trap the geminate pair of atoms arising from a photodissociated molecule, many experiments were performed on this issue. Much of the earlier work concerned with the investigation of the "cage effect" is summarized in a review article by Harris et al.[4] The recombination of two atoms inside a solvent "cage" has been termed "primary" recombination and has to be distinguished from "nongeminate" recombination.[2] The latter term describes the usually much slower diffusive recombination of fragments from different parent molecules. Geminate and nongeminate recombination dynamics are usually observed on distinctly different time scales. The photodissociation and geminate recombination of I_2 in different solvents and matrixes is considered a prototype for the experimental and theoretical investigation of an excited-state condensed-phase chemical reaction. While the lifetimes of the excited B state dynamics of free I_2 molecules were found to be on a microsecond time scale,[5] in solution the decay of this state takes place within several hundred femtoseconds.[6] The geminate recombination due to the cage effect in different liquid environments was found to take place within less than 2 ps.[4,7] Recently, experiments have been performed on iodine in different environments with a higher time resolution. Femtosecond experiments were performed on I_2 in rare gases at high pressures,[8−12] in rare gas clusters,[13−15] in solid rare gas matrixes,[16−18] in liquids,[6,19] and in confined nanocavities in water solutions.[20]

A considerable amount of information could be drawn from these experiments which elucidate many aspects of the recombination of the atoms due to the cage effect. The actual diatomic potential energy surfaces (PES) affect rates and pathways of the photodissociation as well as the geminate recombination reactions. The caging may result in (i) trapped excited-state molecules which relax to the ground state by radiative or nonradiative transitions or (ii) ground-state molecules which are formed immediately upon recombination or after surface hopping from excited states. The molecules are formed hot and lose their energy by vibrational relaxation. Most of the experiments cited above were performed using a time-resolved pump−probe technique. The pump laser excites the molecules and the dynamics are followed by a probe laser, detecting laser-induced fluorescence (LIF), ions or transient absorption. With these experiments, it is possible to follow the reaction coordinate beyond the Franck-Condon region, which can be vertically accessed. The spatial coherence of the initially prepared wave packets is measured.[21] In condensed media, these phase coherences are usually lost on time scales of fewer than 100 fs. Therefore, in most cases, spectroscopy in the frequency domain does not yield any vibrational resolution for the excited electronic states.[22−24] To learn more about the chemically relevant processes which play a role for the interaction between excited molecules and/or molecular fragments with the bath, the elementary dynamics have to be observed on a time scale of picoseconds or less. Depending on the pump wavelength, different PES are accessed in I_2 resulting in clearly different (pre-) dissociation, caging, and recombination dynamics.

* To whom correspondence should be addressed.

† This paper is dedicated to Professor Dr. H. Werner, University of Würzburg, on the occasion of his 65th birthday. We admire his extraordinary contributions to chemistry and his remarkable personality. All the best for the future!

‡ Universität Würzburg.
§ Universität Hannover.
|| Karl−Franzens-Universität Graz.

10.1021/jp990111o CCC: $18.00
Published on Web 04/30/1999

Apkarian and co-workers[17−18] prepared wave packets on the repulsive wall of the A state of I_2 embedded in cryogenic matrixes of Ar and Kr ($\lambda_{pump} \approx 640-740$ nm). They probed the time evolution of this wave packet via LIF from the ion-pair states. In contrast to frequency domain experiments, they were able to obtain the dynamics of the coupled molecule−bath system in real time. Most interestingly, they observed that after cage-induced recombination the coherence in the vibrational motion of the I_2 bond lasted for several picoseconds before geminate recombination into the A state took place. This means that after the initial impulsive stretch of the I−I bond (dissociation) collisions of the atoms with the cage wall result in recoil and recombination. In this process, the phase coherence survives, resulting in subsequent coherent oscillations of the nascent I_2 molecule. On the basis of these experiments, Li et al. define recombination as "the permanent vibrational deexcitation of the I_2 molecule below its gas-phase A state dissociation threshold".[18] Wang et al.[14] reported similar coherent behavior also after A state direct dissociation for I_2 molecules in Ar clusters.

Comparable observations were reported by Zewail and co-workers[12] for direct B state dissociation of I_2. They used pump pulses with a wavelength of ∼496 nm to excite I_2 molecules in low-pressure rare gases (≤50 bar). With these pump pulses, wave packets were prepared above the dissociation limit of the B state. The caging that took place under bimolecular, single-collision conditions resulted in "collisional confinement with the atoms not reversing their momentum, caging at shorter internuclear separations, and caging coherently".[12] The solute atoms do not separate completely. Instead, they are caged very rapidly by a single collision with the solvent. Therefore, despite the random nature of the interaction, the coherence is preserved, giving rise to coherent B state oscillations.

For pump wavelengths in the range of approximately 500−620 nm, the absorption of I_2 from the ground X state is dominated by the optical transition to the bound region of the excited B state.[25−28] Experiments in rare gas clusters[13,14,29] as well as in supercritical rare gases (at high pressures, <3 kbar)[8−11] have investigated the dynamics of I_2 molecules excited in such a way. Ultraviolet transient absorption (∼300−400 nm, depending on the solvent shift of the ion-pair states[24,30]) of the excited molecules to ion-pair states occurs from three regions: (i) the B state, (ii) the A/A′ states in their bound region, and (iii) the A/A′ as well as the X states close to their dissociation limits;[31] in each case, detection of LIF from the strong A′ ← D′ is possible.[10,11] The experiments demonstrated that, for higher solvent densities, vibrational relaxation followed by predissociation rapidly depopulates the B state of the I_2 molecules (rate ∼1 ps^{-1}). The repulsive states populated by predissociation have not been conclusively identified. Most probably, the $a1_g(^3\Pi)$ and/or the $a'0_g^+$ ($^3\Sigma^-$) states are involved;[32] others[33] consider the $B''1_u(^1\Pi)$ state as the most important exit channel. Geminate recombination onto the A/A′ states is observed to take place within a few picoseconds. In the high-pressure experiments, it could clearly be shown that both primary (within the solvent cage; fast) and secondary recombination (diffusive; slow) are responsible for the restoration of the I_2 molecule. In contrast to the experiments, where direct dissociation from the A state continuum preceded the caging, no coherent oscillation of the nascent molecules in the A/A′ states could be detected after the predissociation from the bound B state. Additionally, it was concluded from the transient shapes that fluorescence from molecules recombining onto the X state did not significantly contribute to the overall transient signal.

In the experiments discussed in the present paper, we applied a pump wavelength which is resonant with a transition to the bound region of the B state of I_2. We embedded the I_2 molecules in porosils[34−36] which have a microporous structure similar to those of zeolites. The application of crystalline microporous materials as well-defined host components for the modular assembly of new host−guest compounds, for the stabilization of otherwise unstable species, or the topology-controlled arrangement of guest molecules offers an interesting route to novel, nanostructured, solid-state materials.[37,38] From a spectroscopic point of view, a highly interesting aspect of these rigid solid-state matrixes is the opportunity to use these materials as "solid-state solvents" for sufficiently small molecules and to study the behavior of the latter spectroscopically in comparison to that in a liquid solvent. In this respect, porosils, a special class of microporous frameworks consisting of corner-sharing [$SiO_{4/2}$] tetrahedra only, are well-suited compounds. Due to the electroneutrality of the host framework, host−guest interactions are significantly reduced for insertion compounds based on these hosts when compared to analogous composites based on zeolites (which consist of negatively charged aluminosilicate frameworks and charge-compensating cations).

Among the porosils known, we have chosen decadodecasil 3R (DDR)[39] for matrix isolation studies of iodine inserted in the voids of this compound. This is due to the unique host topology which allows one to arrange the guest molecules in a three-dimensional periodic array but isolated from each other in separate cages thus preventing interaction between them.[34,35] The structure of DDR consists of pseudohexagonal sheets of pentagondodecahedra stacked in an ABCABC sequence (panel a of Figure 1).[40] These sheets are connected by further [$SiO_{4/2}$] tetrahedra, whereby cages characteristic of the DDR structure are created (panel b of Figure 1). Each [$4^3\,5^{12}\,6^1\,8^3$] cage with a free volume of around 350 $Å^3$ is surrounded by three other ones (panel c of Figure 1). After hydrothermal synthesis, these cages are filled with a so-called structure-directing agent (here 1-aminoadamantane) which is incorporated during crystallization. However, the organic molecules can be burned out by calcination (treatment in ambient atmosphere at elevated temperatures) leaving an electroneutral SiO_2 modification behind. The crystalline matrix obtained in this way is an excellent basic component for the assembly of new host−guest compounds. Inorganic guest molecules, like iodine,[34,35] mercury halides,[36] or chalcogen molecules,[36,41] have been inserted into this rigid crystalline microporous SiO_2 modification.

The paper is outlined as follows. In the following section, we give a brief discussion of both the experimental arrangement used for the femtosecond time-resolved pump−probe spectroscopy and a description of the sample preparation. Some preliminaries are discussed in the third section. We present the experimental results in the Results section and discuss them in the following section in comparison to former studies on I_2 caging. We summarize our findings at the end of this paper.

2. Experimental Section

A. Experimental Setup. The experimental apparatus for the femtosecond pump−probe experiments has been described in detail elsewhere.[42−44] Briefly, a Ti:sapphire laser system in combination with two four-pass OPAs was used to create the femtosecond pump and probe pulses at variable wavelengths. The wavelength of the pump laser was chosen to be 535 nm for all experiments presented in this paper. The wavelength of the probe laser was varied between 300 and 400 nm. The pulses had energies of several μJ and durations of typically 80 fs at a

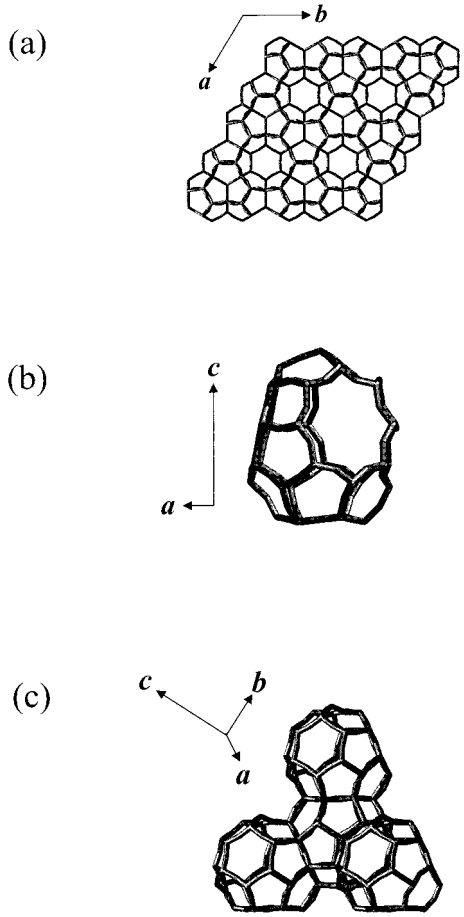

Figure 1. In (a), a view along the crystallographic *c* axis is given, showing the sheets of pentagondodecahedra. By connecting these sheets by further [$SiO_{4/2}$] tetrahedrons, the [$4^3 5^{12} 6^1 8^3$] cages characteristic of the DDR structure are built up between them (b). Each [$4^3 5^{12} 6^1 8^3$] cage is surrounded by three adjacent cages in an angle of 120° (c).

repetition rate of 1 kHz. The pulses were delayed relative to each other by means of a Michelson interferometer arrangement. The relative timing between the two pulses was varied with a high-precision, computer-controlled actuator located in the path of the pump laser. Pump and probe pulse were made collinear and focused on the sample with the help of an achromatic lens. The scattered probe light was collected by means of a Cassegrain telescope, spectrally filtered with the help of a monochromator, and finally detected by a fast photomultiplier tube. The change in the intensity of the scattered light due to transient absorption was measured using a combination of a lock-in amplifier (locked to the chopping frequency 127 Hz of the pump laser light) and a boxcar integrator. The transient signal was recorded as a function of actuator position. The I_2−DDR powder was fixed on a small sample holder which could be adjusted in the *x*-, *y*-, and *z*-directions.

B. Sample Preparation. The hydrothermal synthesis of DDR was performed as follows. In 10 mL (556 mmol) deionized H_2O was suspended 0.504 g (3.38 mmol) of 1-aminoadamantane. After the solution was stirred for 15 min, 0.822 g (22 mmol) NH_4 F were added and the resulting mixture was stirred for further 10 min. In the next step, 0.15 mL (3.4 mmol) of 40 wt % HF were added to the homogeneous suspension. Finally, 1.33 g (22 mmol) SiO_2 (Cab-osil M-5, Fluka) were mixed into the suspension, whereby all the SiO_2 was added in one part. The highly viscous gel was homogenized by stirring for 1 h. Thereafter, the gel was filled into a home-built, Teflon-lined autoclave (degree of filling 80%). For crystallization, the closed autoclave was held in a forced-air oven at 433 K (temperature constancy 1 K) for 21 days. After the autoclave was allowed to cool to room temperature, the crystals were filtered off and washed with diluted NaOH and finally deionized H_2O in order to remove amorphous gel residues. The calcination process was performed by heating the crystals to 1123 K within 10 h, holding them at this temperature for 4 h, and finally cooling them to room temperature within 24 h. After calcination, the crystals were colorless as was the as-synthesized product. The crystallinity and phase purity of both the as-synthesized and calcinated products were confirmed by powder X-ray diffraction.

Insertion compounds of iodine in DDR were prepared in 10 mL autoclaves. The host compound was placed in a small glass tube on the top, whereas iodine was on the bottom in order to avoid a deposition of bulk iodine on the host surface during cooling of the autoclave. For products obtained using typical reaction conditions (3 days, 433 K), thermal analysis on a Mettler TA 2 (heating rate, 10 K min^{-1}; atmosphere, Ar; flux rate, 5 L h^{-1}, reference, Al_2O_3; crucible material, Al_2O_3) yielded a composition of $120SiO_2 \cdot 6.0I_2$, i.e., every cage is occupied by just one iodine molecule. Thermal analysis revealed the composition to remain unchanged regardless if the host was used in the form of a crystals or as a powder. Hence, it is justified to assume the contribution of iodine located at the outer surface to be negligibly small. Furthermore, we would like to point out that the porosils are hydrophobic and therefore it was not necessary to keep the samples under anhydrous conditions.

3. Preliminaries

In the femtosecond experiments on iodine[11] or sodium iodide[43] in high-pressure rare gas environments, a pump−probe technique combined with the detection of laser-induced fluorescence (LIF) was applied. However, LIF detection turned out not to be favorable in the case of the experiments on porosils. Porosils doped with I_2 are dark red and show a strong absorption of light over a wide spectral range.[34,35] Due to the high concentration of I_2, considerable transient absorption also takes place, giving rise to very efficient reabsorption of the LIF light. As the powdered samples are not transparent, a transient absorption measurement cannot be performed in the common way. To probe the wave packet motion in the excited electronic states, we focused pump and probe lasers on our sample and detected the probe light which was scattered from the I_2−porosil composite. The constant background of scattered light was suppressed, and the intensity changes due to the resonant interaction with the excited I_2 molecules were monitored by using the lock-in technique. In our experiments, we modulated the pump laser and then locked to the chopper frequency. For convenience, we will present the so-measured transients in a way comparable to the transients obtained by means of LIF detection by inverting the course of the intensity change. The decrease of scattered light intensity will be shown as an increase of the displayed transient curve.

In Figure 2 the potential curves of I_2 which are involved in the dissociation−recombination process are displayed. The equilibrium molecular I_2 absorption spectrum peaks around 500 nm and extends to 700 nm. Excitation within this absorption results in population of the A/A′, B″$1_u(^1\Pi)$, and B states. For wavelengths within the red wing of the I_2 absorption (600−700 nm), the A/A′ states are populated above their dissociation limit, while for wavelengths shorter than 600 nm most of the population is transferred into the B state.[27,28] In our experiments, the pump pulse at $\lambda_{pump} = 535$ nm primarily prepares a wave packet within the bound B state. The atoms move apart after

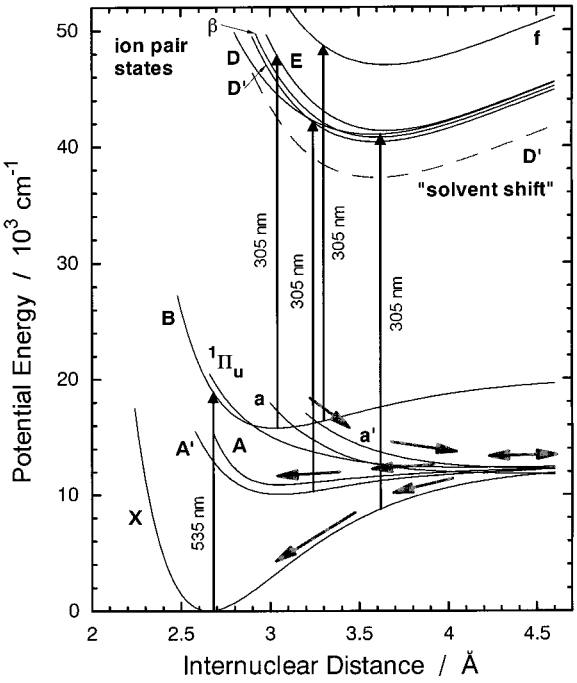

Figure 2. Potential energy curves of I_2. Vertical arrows indicate optical transitions. A pump laser pulse at 535 nm is used to excite the I_2 molecule by an optical transition B ← X. Typical probe transitions are shown for $\lambda_{probe} = 305$ nm. The dashed line shows the solvent shift of the D′ ion-pair state estimated from the experimental results. The thick arrows indicate the predissociation (here, assuming coupling of the B state onto the repulsive a′ state) and possible recombination paths.

predissociation and recombine due to the solvent cage. Predissociation and recombination within dense solvent cages are essentially completed within a time on the order of 1 ps.[13] The so-formed molecule undergoes vibrational relaxation, following the crossing to the A/A′ as well as ground-state X potentials. The probe wavelength determines the window in which the wave packet is viewed. In most cases, a longer probe wavelength is equivalent to probing longer distances of separation but might also result in probing different potential energy surfaces.[11,45] For I_2, absorption from the X state is dominated by optical transitions to the B state in the visible to near-infrared region. In the ultraviolet, absorption to ion-pair states occurs from two regions: the stable A/A′ state potential well and regions of the X and A/A′ states near their dissociation limits (compare Figure 2). The A and A′ states have well depths of 1640 and 2500 cm^{-1}, respectively, for free gaseous iodine.[46−48] The radiative lifetimes of these states in rare gas matrixes are very long in comparrison to the time scale of our experiments (A state, 143 μs; A′ state, 6 ms).[24] The vibrational relaxation of molecules that recombine onto the X state potential is monitored best through the B−X absorption.[4] In solvents it shifts continuously from the near-infrared to its equilibrium peak at 500 nm as the molecule vibrationally relaxes within 50−150 ps.[7,31] The branching ratios for ground state versus A and A′ state recombinations depend on solvent viscosities and are close to 1 in each case.[31]

For iodine in Ar clusters,[14] in rare gas matrixes,[17,16] and in other solvents, such as, e.g., high-pressure rare gas,[8,10,11] a red shift of the LIF emission was observed. This shift can be assigned to the lowering of the ion-pair states relative to the valence states due to solvation.[30] For I_2 embedded in the porosils, we assume that the solvation effect simply decreases the potential energy of the ion-pair states by a value similar to that observed for $I_2 \cdot Ar_n$ (4200 cm^{-1})[14] or I_2 embedded in rare gas matrixes (5600 cm^{-1}).[17] Compared to free I_2, the maximum absorption shifts to lower vibrational levels for equivalent probe wavelengths. For example, at 305 nm, the optimal absorption is centered near the potential minima of the A/A′ states.

4. Results

In this section, we present the results obtained from a series of experiments on I_2 occluded in the porosil DDR at room temperature (∼295 K). Ground-state I_2 molecules were excited with 535 nm. We will discuss transients taken with probe laser wavelengths at 305, 322, 352, and 400 nm which best display the characteristic changes observed for this wavelength range. In each transient, time zero was fixed to the time at which the initial rise of the signal reaches half of its maximum of the signal change due to B state absorption. At each probe wavelength, we recorded scans over different time intervals with different time delays between adjacent data points. To determine the B state contributions short scans with relatively high resolutions were always used. For each data point we accumulated up to 10 000 laser shots. Each transient measurement was repeated several times and averaged afterward (up to 10 repetitions). The transients were taken from different sample spots without considerable changes of the transient shapes.

In Figure 3 the four transients are displayed. For $\lambda_{probe} =$ 400 nm, the signal in panel a shows a rapid rise giving the cross correlation of the pump and probe lasers. The following exponential decay has a time constant of 0.33 ps^{-1}. The signal reflects the excitation of the B state and the subsequent decay due to collision-induced electronic predissociation. We assume the probe wavelength at 400 nm to be close to the "cutoff wavelength" for detection of the recombined iodine molecules for two reasons: (i) we could not detect a signal after the B state was completely depopulated and (ii) only a very small residual signal remained at early time delays (10−30 ps) after subtracting the single-exponential fitting curve (thick line in panel a of Figure 3).

From the high-pressure experiments[11] we know that for a certain pressure the B state population decay is independent of the probe wavelength. To simplify the transients for $\lambda_{probe} =$ 352, 322, and 305 nm we subtracted the B state contribution assuming the decay constant obtained from the 400 nm transient. As an example we show in Figure 4 the transient for $\lambda_{probe} =$ 322 nm before (dashed line) and after (solid line) B state subtraction. The insert displays the uncorrected transient obtained with a higher resolution (50 fs steps). The B state signal can clearly be resolved. All transients shown in the following were treated in the same way. This means that only signals due to the cage effect are displayed.

Panel b of Figure 3 shows the transient signal obtained for a probe pulse centered at 352 nm. The transient was taken over a time interval of 100 ps with a step width of 1 ps. The signal rises to a maximum and slowly decays. At 100 ps, only a small intensity change of the scattered probe light could be detected which vanishes for longer delay times (not shown here). The signal rise which starts about 1−2 ps after time zero is due to the recombination of the iodine atoms ("recombination signal"); the decay reflects the vibrational relaxation through the probe window that is centered at high vibrational levels of A/A′ and X states. The B state signal which was subtracted from the transient had an intensity comparable to the remaining signal.

The B state signal detected for $\lambda_{probe} = 322$ nm only had approximately half of the intensity of the recombination signal (compare Figure 3) and that of the 305 nm transient was at the limit of a detectable signal. The signal for 322 nm is displayed

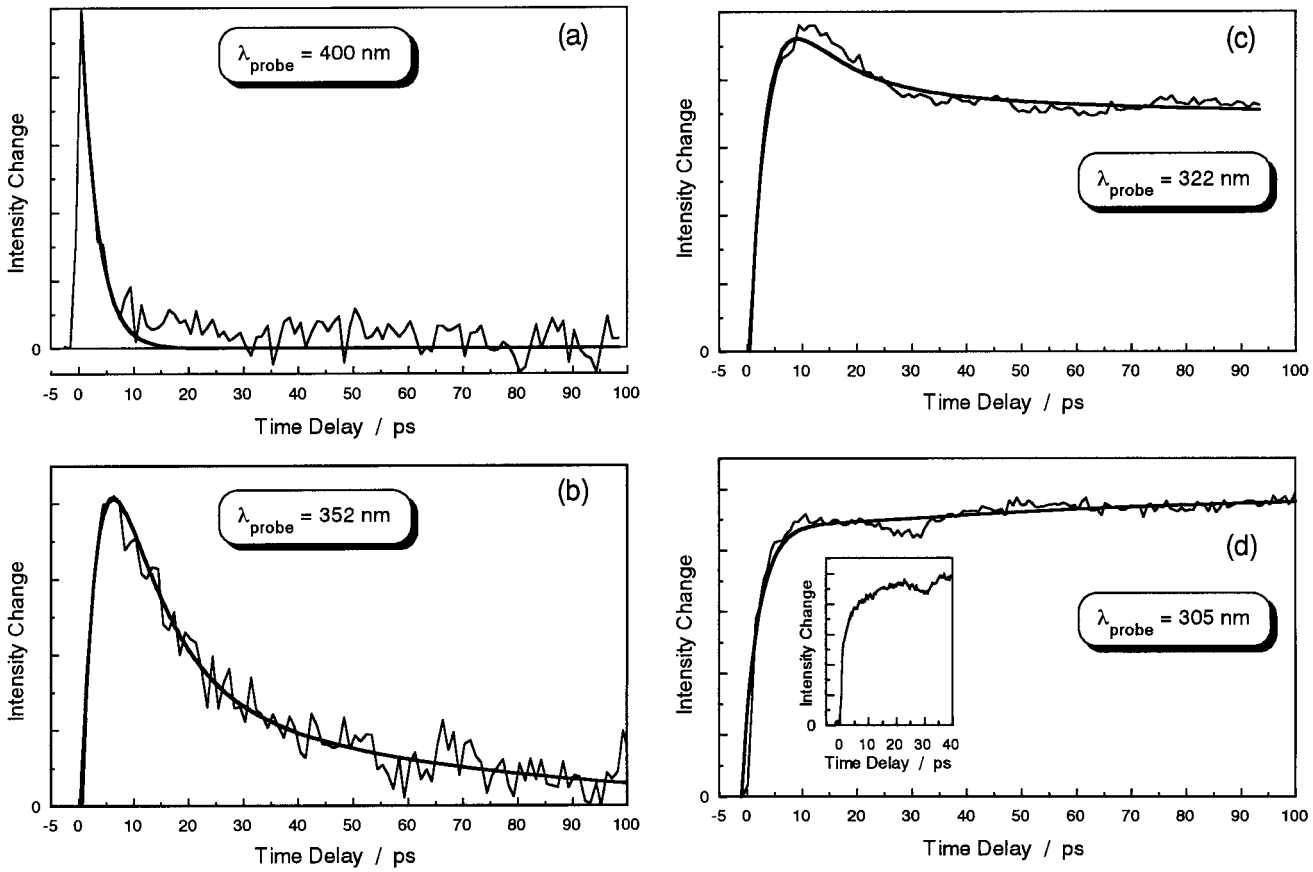

Figure 3. Transients of I_2 in DDR observed for a pump laser wavelength of 535 nm and different probe laser wavelengths. (a) $\lambda_{probe} = 400$ nm: the signal decay due to predissociation of the B state dominates this transient. The fitted line (smooth line) was obtained using the single-exponential decay $a \exp(-k_{pred}t)$. The other panels show transients after subtraction of the predissociative signal. The signals were measured using (b) $\lambda_{probe} = 352$ nm, (c) $\lambda_{probe} = 322$ nm, and (d) $\lambda_{probe} = 305$ nm. The insert in panel d shows a transient taken with higher resolution to demonstrate the reproducibility of the feature between 30 and 40 ps. The smooth lines are the results from a simulation of the experimental data with the expression given in eq 4 (only geminate recombination).

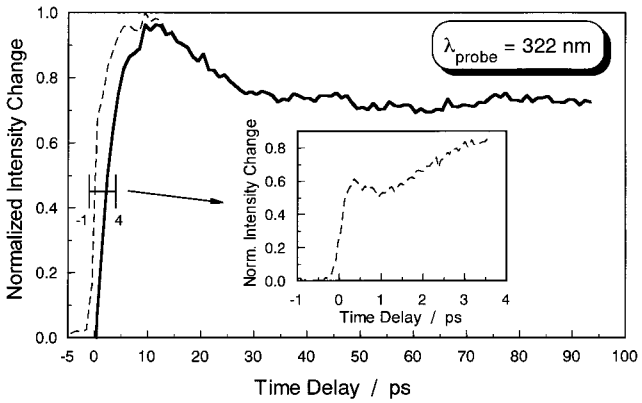

Figure 4. Demonstration of the subtraction of the signal resulting from the predissociation of the B state of I_2 from the measured transient obtained for a probe laser wavelength $\lambda_{probe} = 322$ nm. The experimentally obtained curve is shown by the dashed line. The full line represents the transient after subtraction. The insert displays the experimental transient for early time delays recorded with a better time resolution.

in panel c of Figure 3. Again, the transient is shown over a time interval of 100 ps. The resolution was 1 ps per time step. Similar to the 352 nm transient, the recombination signal rises only approximately 1 ps after time zero and then decays slowly. In contrast to the red-shifted probe wavelength at 352 nm, the signal does not completely vanish after a few hundreds of picoseconds but stays nearly constant (or only slightly rises) after about 50 ps.

This behavior becomes even more obvious for $\lambda_{probe} = 305$ nm. Here, the signal decay is very slow and only lasts for approximately 30 ps. After this, the signal suddenly rises within less than 10 ps to a level higher than the first maximum at about 10−20 ps. Finally, the intensity change of the scattered probe light is found to increase with a small time constant over the whole accessed time range. The 305 nm transient was taken with time steps of 0.7 ps. The insert displays a shorter transient taken with better resolution (0.3 ps) in order to demonstrate the reproducibility of the "dip" at about 30 ps.

5. Discussion

Comparing the results presented in the previous section with results obtained in high-pressure rare gases[10,11] yields many agreements but also some differences which we will discuss in the following. If not stated otherwise, for comparison we use results from the paper by Materny et al.[11] which describes "probing along the reaction coordinate and dynamics in supercritical argon" for the system I_2 in Ar at high pressures.

The fast rise and decay of the "B state contribution" in the transients reflects the excitation of I_2 into its bound B state and the subsequent decay due to the predissociation. The presence of the matrix induces couplings between the bound B state and several repulsive states which cross the B state. These couplings are responsible for the predissociation of the excited molecules via different exit channels. Tellinghuisen[49] assumed that on the basis of symmetry arguments the $B''1_u(^1\Pi)$ state is unimportant for predissociation compared to the $a1_g(^3\Pi)$ and $a'0_g^+(^3\Sigma^-)$

states. However, recently, Raman studies of I_2 in liquid xenon yielded results which favor the $B''1_u(^1\Pi)$ state predissociation channel.[32,50] This is in agreement with the results of calculations using a coupled quantum classical molecular dynamics method.[33] This model predicts that the $B''1_u(^1\Pi)$ state plays the most important role in the nonadiabatic relaxation of the excited B state. However, at high solvent densities, other states, such as the above-mentioned $a1_g(^3\Pi)$ and $a'0_g^+(^3\Sigma^-)$ states, can also play a role in B state deexcitation.

Scherer et al.[6,51] found in their time domain measurements of optically induced dichroism of I_2 in solution that probe absorptions from predissociative states are first observed at approximately 150 fs after excitation by the pump laser. Predissociative absorptions to the ion-pair states are typically 10 times more intense than B state absorptions terminating in the same final states. Therefore, in the condensed phase, I_2 molecules excited into the B state obviously couple onto repulsive states within half a B state vibrational period. The "B state contributions" seen in our transients should be termed more precisely as "predissociative contributions". As mentioned in the previous section, these early contributions to the transients were subtracted, leaving only the temporal changes due to recombination dynamics. The subtraction was carried out using the (appropriately scaled) single-exponential decay which we obtained from the transient obtained for $\lambda_{probe} = 400$ nm (panel a of Figure 3). The assumption that the decay does not depend on the probe wavelength seems to be reasonable, especially when one considers the signal to be dominantly arising from the coupling repulsive states. Using $a \exp(-k_{pred}t)$ to fit the decay resulted in a predissociation rate k_{pred} of 0.33 ps^{-1}. This value is comparable to the value obtained for an Ar pressure between 200 and 400 bar in the high-pressure experiments (0.25 and 0.45 ps^{-1}, respectively). The mean free path of I_2 molecules in argon at 200 and 400 bar is approximately 12 and 4 Å, respectively. The volume of a porosil cage is ~350 $Å^3$. Hence, with regard to the predissociation, a comparison between the high-pressure conditions and the solid cages seems feasible. Information on the effect of the solvent could also be obtained from experiments on iodine in high-pressure rare gases by Lienau et al.[9,10] Comparing different rare gases (He, Ne, Ar, Kr), the authors found that the reaction cross section per collision increases drastically with increasing size of the solvent atom. A considerable similarity between the results at liquidlike densities and those from a study by Capelle and Broida[5] at a pressure of only 4×10^{-5} bar point to the fact that binary collisions are responsible for the bond breaking even at high solvent densities. The comparison between our results and those obtained in other systems (as discussed above) shows that in DDR binary collisions also seem to induce the predissociation of the I_2 molecules.

Similar to the findings of the high-pressure experiments, we observed a "cutoff wavelength". Only up to this limiting probe wavelength a signal from recombined I_2 molecules could be detected. If the probe laser wavelength is tuned further to the red, the transient is solely determined by the predissociative contribution arising from the predissociation of the originally excited B state. The cutoff wavelength for I_2 embedded in DDR is approximately 400 nm. In supercritical Ar this wavelength depends on the argon pressure and changes from ~360 nm at 800 bar to ~380 nm at 2500 bar. Obviously, the red shift of the ion-pair states is close to that observed for I_2 embedded in rare gas matrixes (5600 cm^{-1}).[17]

After subtracting the predissociative contribution from the transients, the recombination signal remains. It can be assumed that no signal arises from X state molecules. As vibrational relaxation on the X state takes about 100 ps for the population to move out of the probe window,[15,52] rise and decay features in the transients should have been observed. However, none of the transients taken in the course of our experiments showed any decay on this rather long time scale. Therefore, we conclude that, consistent with the work on both matrix[14] and high-pressure systems[10,11] X state contributions do not have any importance for the interpretation of the transients.

Transients displaying predissociation and recombination of I_2 molecules in high-pressure rare gases show a damped oscillatory modulation of the fluorescence signal, which reflects the dephasing of the coherent vibrational motion of the wave packet. The rare gas collisions induce a dephasing of the coherences. While for He and Ne the coherent motions can be observed up to the highest pressures, no oscillations can be detected in Ar and Kr at pressures higher than about 200 bar. In the iodine−porosil system, no oscillatory modulation of the transients could be observed at all. This points to a very efficient dephasing of the coherent wave packet motion due to collisions with the surrounding solid cage. Oscillations which were observed in solid rare gas matrixes[16−18] as well as in clusters[14] after excitation into the repulsive branches of the A/A′ states cannot be observed after predissociation. The coupling of the B state onto (different) repulsive states followed by caging obviously destroys the coherence while direct dissociation and recombination preserve it. For the iodine−porosil system, experiments with different pump wavelengths are in progress.

To enable us to compare our experimental results with the results discussed in ref 11, a simple kinetic model will be considered in the following. This model takes the elementary steps of the reaction into account. For convenience, the same abbreviations as in the paper by Materny, Lienau, and Zewail[11] will be used here. As the pump wavelength applied in our present work mainly results in B state excitation, we neglect adiabatic recombination resulting from molecules that are originally excited into the repulsive branch of the A state. The nonadiabatic process is described by the predissociation of the B state population onto the repulsive states (in the model we will use "a" to designate the possible reaction paths), the caging, the formation of molecules in the high vibrational levels (A*) of the A/A′ state potentials, and finally vibrational relaxation to low vibrational levels (A):

$$B \xrightarrow{k_{pred}} a \xrightarrow{c(t),q_{A/A'}} A^* \xrightarrow{k_{VR}} A \qquad (1)$$

Here, $q_{A/A'}$ is the quantum yield of the formation of molecules in the A/A′ states. The function $c(t)$ reflects the distribution of "recombination times", where t is the time delay at which the caging takes place. Using picosecond transient Raman spectroscopy, Lingle et al.[53] investigated the reaction dynamics of iodine geminate recombination on the excited A′ state. Comparing their results obtained for different solvents, they found that the appearance time of the cold vibrational levels of the A′ state is not determined by the rate of vibrational energy relaxation alone. The vibrational energy relaxation measured was found to be significantly slower than that in the ground X electronic state and was shown to be largely dependent on the mass of the solvent with slower relaxation occurring in the heavier solvents. However, the rate of formation of the A′ state was found to be inconsistent with the solvent dependence of the vibrational energy relaxation, which shows that the mechanism of geminate recombination on the A′ state may be fundamentally different than that of the X state. As was argued above, the

caging onto the ground state in our experiments is unlikely to influence the transient signal. Therefore, it seemed to be sufficient to assume a distribution of caging times followed by a relaxation process yielding vibrationally cool molecules in the A/A′ states. In the kinetic model, k_{VR} is the rate constant for vibrational relaxation leading to the vibrationally cold A/A′ states. For the interpretation of the transients discussed in the present paper, this reduction to a two-level relaxation from hot A* to cold A is sufficient. The total intensity change of the scattered probe light $\Delta I(t)$ is given by $\Delta I(t) = a_B[B(t)] + a_{A*}[A^*(t)] + a_A[A(t)]$. The amplitudes a_B, a_{A*}, and a_A are proportional to the absorption cross sections in B, A*, and A, respectively. The differential equations used for the derivation of $\Delta I(t)$ are

$$[\dot{B}(t)] = -k_{pred}[B(t)],\ [B(t)] = B_0,\ [B(t \le 0)] = 0$$

$$[\dot{a}(t)] = -k_{pred}[B(t)] + \int_{-\infty}^{t} [\dot{B}(t')] q_{A/A'} c(t - t')\, dt',\quad [a(t \le 0)] = 0$$

$$[\dot{A}^*(t)] = -\int_{-\infty}^{t} [\dot{B}(t')] q_{A/A'} c(t - t')\, dt' - k_{VR}[A^*(t)],\quad [A^*(t \le 0)] = 0$$

$$[\dot{A}(t)] = k_{VR}[A^*(t)],\quad [A^*(t \le 0)] = 0 \qquad (2)$$

As mentioned before, the predissociative contribution was subtracted from the experimental transients. Therefore, the remaining recombination signal can be described by simply using $\Delta I(t) = a_{A*}[A^*(t)] + a_A[A(t)]$. For the solution of the differential equations, we have to define a model function for the distribution of recombination times $c(t)$. In order for the I_2 to re-form, the iodine atoms have to relax through collisions with the $[SiO_{4/2}]$ framework. In the rigid cages formed by the $[SiO_{4/2}]$ tetrahedra caging should be dominated by rapid primary recombination as observed for experiments in liquid solvents.[4] Due to the confined size of the cages (~350 Å^3), the iodine atoms reach an appropriate internuclear separation for geminate recombination without extensive diffusive motion. This means that no diffusive process outside the solvent cage results in slow geminate recombination ("secondary recombination") of the iodine atoms. Therefore, according to ref 11, we first assume a narrow distribution of caging times, approximated by

$$c(t) = \begin{cases} 0, & t < \Delta t_{gem} \\ k_{gem} \exp(-k_{gem}(t - \Delta t_{gem})), & t \ge \Delta t_{gem} \end{cases} \qquad (3)$$

Here, k_{gem} is the rate constant for geminate recombination and Δt_{gem} is the time delay for the onset of geminate recombination. Using this distribution function, we obtain the following expression for the signal:

$$\Delta I(t) = \sigma_1 \exp(-k_{pred}t) + \sigma_2 \exp(-k_{gem}t) + \sigma_3 \exp(-k_{VR}t) \qquad (4)$$

where the amplitudes σ_1, σ_2, and σ_3 are functions of the rate constants as well as of Δt_{gem}, a_{A*}, and a_A. The rate constants k_{gem} and k_{VR} together with Δt_{gem}, a_{A*}, and a_A are free parameters in the simulations. The transient obtained with a probe wavelength of 352 nm (panel b of Figure 3) was assumed not to depend on the term $a_A[A(t)]$. The signal (intensity change of the scattered probe light) nearly decays completely after only 100 ps. Therefore, the probe window obviously does not include the vibrational cold A/A′ states ("A" in our model). All free parameters were fitted globally to all transients except for amplitudes, which reflect changing experimental conditions as well as the shift in the probe window. The simulations are shown together with the experimental data in Figure 3. While for $\lambda_{probe} = 352$ nm the fit gives good agreement with the experimentally observed transient, the data measured with $\lambda_{probe} = 322$ and 305 nm cannot be reproduced to our satisfaction. If only the short-time dynamics (up to about 20 ps) is fitted, the resulting rate constants are faster and relatively good simulations can be obtained. However, with these parameters the slow rise of the signal in panel d ($\lambda_{probe} = 305$ nm) is not reflected by the calculated curve.

These results are very similar to those reported in ref 11. There, the high-pressure Ar transients also exhibit a slow signal rise at the blue probe wavelength which cannot be correctly described using the narrow distribution of caging times as assumed in eq 3. In supercritical rare gases, recombination occurring on a time scale of hundreds of picoseconds can be explained by assuming secondary recombination. Iodine atoms break out of the solvent cage and recombine diffusively. Also in the clusters, there is clear evidence of extensive cage exit and subsequent diffusion-controlled recombination,[29] while for I_2 in solid rare gases, caging seems to be complete.[16] As mentioned in the Introduction, the cages characteristic of the DDR structure are surrounded by three other ones (compare panels b and c of Figure 1). While I_2 molecules can only diffuse from cage to cage very slowly at high temperatures, iodine atoms should be able to move to a neighboring porosil cage with higher probability even at room temperatures. In rare gas clusters, the average recombination times ranged from 5 to more than 10 ps.[15] Hence, the internuclear separation of the two iodine atoms following predissociation was as great as 9 Å. As each cage of our DDR sample is occupied by one I_2 molecule, within similar time delays, some iodine atoms are able to enter adjacent cages and react with atoms stemming from different I_2 molecules. Certainly, such "nongeminate recombination" would be more probable than a geminate secondary caging process. The nongeminate process depends on the probability of the atom leaving the cage as well as on the probability of this atom finding a dissociated molecule (quantum efficiency of B state excitation and predissociation). We incorporate this slower caging in our model by assuming a distribution function for recombination times, which is charactericed by two rate constants (k_{gem} and k_{ngem} for geminate and nongeminate recombination, respectively).

$$c(t) = \begin{cases} 0, & t < \Delta t_{gem} \\ p_{gem} k_{gem} \exp(-k_{gem}(t - \Delta t_{gem})), & \Delta t_{gem} \le t > \Delta t_{ngem} \\ p_{gem} k_{gem} \exp(-k_{gem}(t - \Delta t_{gem})) + & \\ (1 - p_{gem}) k_{ngem} \exp(-k_{ngem}(t - \Delta t_{ngem})), & t \ge \Delta t_{ngem} \end{cases} \qquad (5)$$

The two contributions are weighted by p_{gem} and $p_{ngem} \approx 1 - p_{gem}$. Δt_{ngem} accounts for the expected longer time delay expected for the onset of nongeminate recombination. The total signal is now given by

$$\Delta I(t) = \kappa_1 \exp(-k_{pred}t) + \kappa_2 \exp(-k_{gem}t) + \kappa_3 \exp(-k_{ngem}t) + \kappa_4 \exp(-k_{VR}t) \qquad (6)$$

where k_{ngem}, p_{gem}, and Δt_{ngem} are additional free parameters in the simulation. The comparison between the experimentally observed pump−probe transients and the simulations using eq 6 is displayed in Figure 5. It is obvious that the consideration of the slower nongeminate recombination improves the simula-

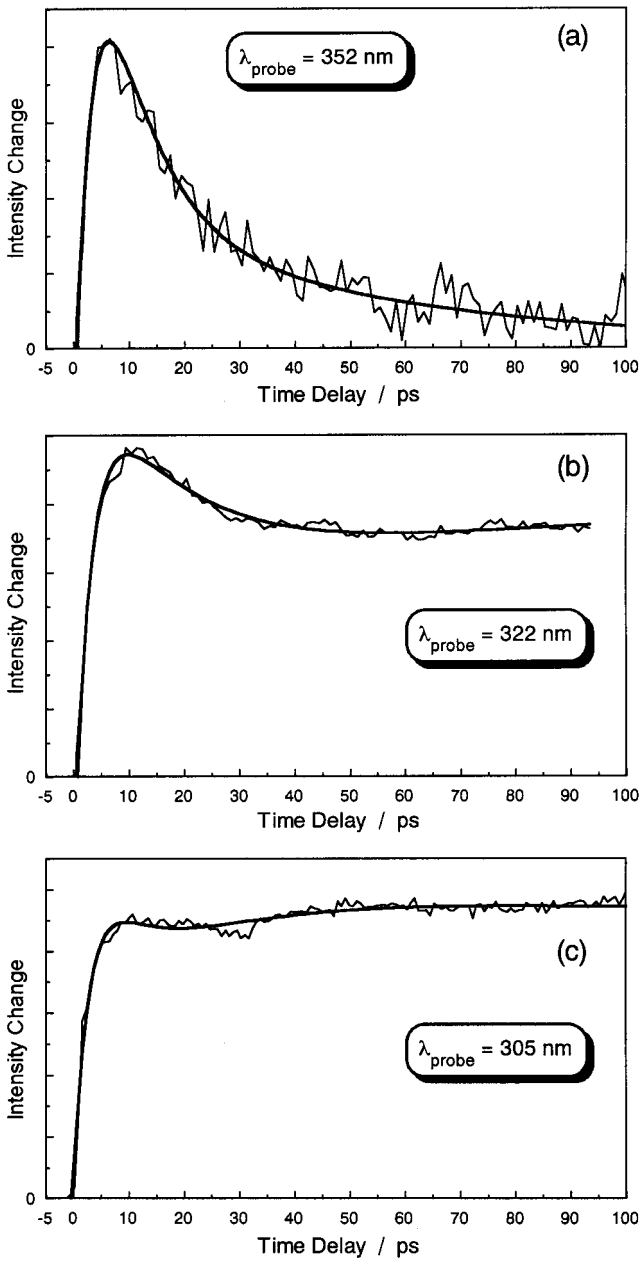

Figure 5. Transients of I_2 in the DDR porosil observed for a pump laser wavelength $\lambda_{pump} = 535$ nm and different probe laser wavelengths. The panels show transients after subtraction of the predissociative signal. The signals were measured using (a) $\lambda_{probe} = 352$ nm, (b) $\lambda_{probe} = 322$ nm, and (c) $\lambda_{probe} = 305$ nm. The smooth lines are the results from a simulation of the experimental data with the expression given in eq 6 (including nongeminate recombination).

tion considerably. This can be best seen from panels b and c where the general agreement between transients and the fitted curves for $\lambda_{probe} = 322$ and 305 nm, respectively, is more accurate than before. The changed fitting function results in only relatively small changes of the old parameter values. As expected, both rate constants k_{gem} and k_{VR} become somewhat faster and are approximately 0.13 and 0.022 ps^{-1}, respectively. The rate constant k_{ngem} for nongeminate recombination was found to be 0.049 ps^{-1}, which is clearly faster than the slow secondary recombination observed in compressed Ar ($k_{cage}^{slow} = 0.003-0.005$ ps^{-1}).[11] This rate corresponds to a time constant $\tau_{ngem} \approx 20$ ps which is exactly the time one would estimate for the transition of an iodine atom from one cage to the other. This is also supported by the value obtained for Δt_{ngem}. While the onset of geminate recombination is already observed after approximately 2 ps (Δt_{gem}) nongeminate recombination starts after about 5 ps. The probability for geminate recombination is considerably higher than that for nongeminate recombination. This is reflected by the parameter p_{gem} for which we determined an optimal value of about 0.9. The parameters obtained from the data analysis are summarized in Table 1. Interestingly, the rate constants for geminate primary recombination (k_{gem}) and vibrational relaxation (k_{VR}) are both close to those values which were determined for I_2 in Ar gas between 200 and 400 bar (200 bar, $k_{cage}^{fast} < 0.17$ ps^{-1}, $k_{VR} = 0.017$ ps^{-1}; 400 bar, $k_{cage}^{fast} = 0.17$ ps^{-1}, $k_{VR} = 0.029$ ps^{-1}).[11] This clearly points to the fact that the mean free path is a determinant parameter for predissociation (see discussion above), recombination, and vibrational relaxation.

TABLE 1: Results Obtained by Fitting the Experimental Transients at All Probe Wavelengths to Eq 6[a]

parameter	fitting result
k_{pred} (ps^{-1})	0.33
k_{gem} (ps^{-1})	0.13
k_{ngem} (ps^{-1})	0.049
p_{gem}	0.9
Δt_{gem} (ps)	2
Δt_{ngem} (ps)	5
k_{VR} (ps^{-1})	0.022

[a] k_{pred} denotes the B state predissociation rate, k_{gem} and k_{ngem} are the rate constants for geminate primary and nongeminate recombination, respectively. p_{gem} is the probability for the geminate process, Δt_{gem} and Δt_{ngem} are the time delays for the onset of geminate and nongeminate recombination, respectively. The rate constant for vibrational relaxation within the A/A′ states is given by k_{VR}.

Comparing the fitting curve with the experimental transient obtained for a probe wavelength $\lambda_{probe} = 305$ nm (panel c of Figure 5), one notices slight discrepancies at time delays between 30 and 40 ps. Here, in the experimental data, a diplike structure occurs which is completely reproducible (compare insert in panel d of Figure 3). Upon a closer look at transients obtained from I_2 in supercritical Ar one finds similar features at approximately the same time delays. In Figure 6, two examples are reproduced from data published in ref 11. We do not have a conclusive explanation for this behavior. It might be caused by a ground X state contribution, which we rule out; X state relaxation should take place on a longer time scale. In our model, the predissociation was simplified by only considering one repulsive potential. However, as discussed above, three such potentials might be involved in this process giving rise to a more complicated distribution of recombination times. A further simplification was already discussed in ref 1. At blue wavelengths, I_2 is probed in vibrationally relaxed and intermediate vibrational levels on the A/A′ states with similar weight. The assumption of a two-level system A* and A with a single-exponential relaxation rate could be too crude an approximation. However, the consideration of the dependence of the vibrational relaxation rate on the vibrational energy seems not to be reasonable in our case, as it would introduce too many new parameters. Therefore, we have to leave this question open for further investigations.

6. Summary and Conclusions

In this contribution, we report the ultrafast dissociation and recombination dynamics of I_2 enclosed in solid cages. The microporous material used in our study as the "crystalline solid-state matrix" for the I_2 molecules was the porosil decadodecasil 3R (DDR). The cages are formed by corner-sharing [$SiO_{4/2}$] tetrahedrons only, resulting in an electroneutral host framework,

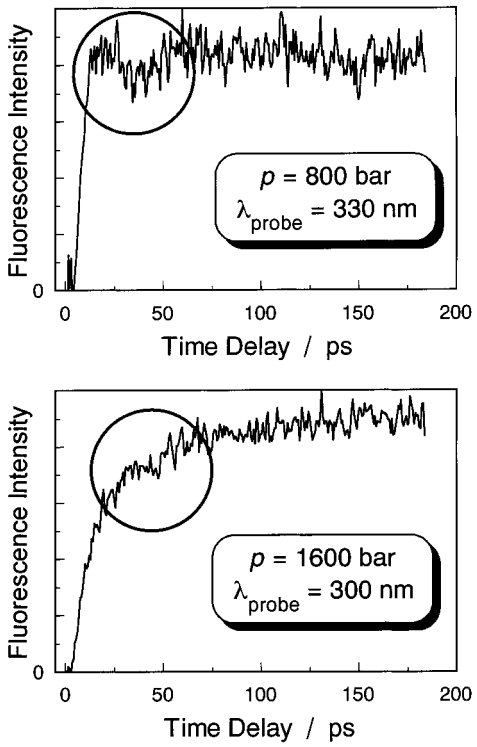

Figure 6. Transients of I_2 in compressed supercritical Ar at different pressures observed for a pump wavelength $\lambda_{pump} = 620$ nm and different probe wavelengths. Pressures as well as probe wavelengths are indicated in each panel. The feature which is discussed in the text is emphasized by circles. The figure reproduces data already published in ref 11.

where host−guest interactions are significantly reduced. In this compound, just one I_2 molecule is located in each case. Hence, the iodine density was much higher than in recent investigations of I_2 in rare gases at high pressure[10,11,54] or solid rare gas matrixes.[16−18]

In a femtosecond pump−probe experiment, a pump laser at 535 nm was used to resonantly excite the I_2 molecules into their bound B state. The collision-induced B state predissociation as well as the recombination dynamics were followed by the time-delayed probe laser pulse. Variation of the probe laser wavelengths (305−400 nm) allowed for opening windows at different positions along the reaction coordinate. With this tunability, we were able to interrogate the different steps starting from the separation of the iodine atoms up to the complete reformation of the I_2 molecules. Instead of observing the laser-induced fluorescence from the ion-pair states, we detected the intensity change of the scattered probe laser light due to transient absorption. Our findings were compared with former results obained for the system of I_2 in Ar gas at high pressures.[11] For this purpose, a kinetic model was used for simulation of the experimental data. It could be shown that, in principle, the same dynamics takes place in the microporous DDR crystals as in the compressed rare gases. After predissociation, the atoms very efficiently lose their kinetic energy through (binary) collisions with the surrounding cage walls. The transients indicate that the intensity changes of the scattered probe laser light originate primarily from I_2 molecules recombining onto the A and A′ state potentials. No contribution could be observed which could be attributed to a recombination onto the ground X state. The recombination dynamics were found to depend on the predissociation rate (k_{pred}), the distribution of recombination times, and the vibrational relaxation rate within the A/A′ states (k_{VR}).

First we assumed a purely geminate primary caging. The recombination was described by a narrow distribution of recombination times, characterized by a rate for fast geminate recombination (k_{gem}). However, with this assumption the experimental transients could not be reproduced satisfactory. Since geminate secondary recombination (diffusive recombination of the atoms after leaving the cage) was likely to be a negligible process in the rigid cages, nongeminate recombinations with atoms stemming from neighboring cells were assumed to contribute to the total recombination process. Since adjacent porosil cages are connected by an opening large enough to permit free access to iodine atoms, this assumption seems to be reasonable. Introducing a slower rate for this nongeminate recombination (k_{ngem}) resulted in a good agreement between simulations and experimental data. The ratio between geminate and nongeminate recombinations was determined to be 0.9. The rate constant for the nongeminate process coincides very well with the mean time one would expect for an atom to move to the neighboring cell and react with another free iodine atom ($k_{ngem} = 0.049$ ps^{-1}). The other rates ($k_{pred} = 0.33$ ps^{-1}, $k_{gem} = 0.13$ ps^{-1}, $k_{VR} = 0.022$ ps^{-1}) are nearly identical to those observed for I_2 in Ar at 200−400 bar. Again, this seems to be reasonable as the mean free path under latter conditions is about the same as that within the DDR cages.

To support our model, further experiments are planned. Additionally, quantum mechanical calculations on the predissociation and recombination dynamics are in progress. As many different zeosil topologies are known, further experiments will also focus on the dependence of the reaction dynamics on the precisely defined geometries of these host materials.

Acknowledgment. This work was funded by the Deutsche Forschungsgemeinschaft (Schwerpunktprogramme "Zeitabhängige Phänomene und Methoden in Quantensystemen der Physik und Chemie", Projekt MA 1564/3-2, and "Nanostrukturierte Wirt−Gast−Systeme", Projekt BE 1664/6-1). Support by the Fonds der Chemischen Industrie is gratefully acknowledged.

References and Notes

(1) Franck, J.; Rabinowitch, E. *Trans. Faraday Soc.* **1934**, *30*, 120.
(2) Rabinowitch, E.; Wood, W. C. *Trans. Faraday Soc.* **1936**, *32*, 547.
(3) Rabinowitch, E.; Wood, W. C. *Trans. Faraday Soc.* **1936**, *32*, 1381.
(4) Harris, A. L.; Brown, J. K.; Harris, C. B. *Annu. Rev. Phys. Chem.* **1988**, *39*, 341.
(5) Capelle, G. A.; Broida, H. P. *J. Chem. Phys.* **1973**, *58*, 4212.
(6) Scherer, N. F.; Jonas, D. M.; Fleming, G. R. *J. Chem. Phys.* **1993**, *99*, 153.
(7) Harris, A. L.; Berg, M.; Harris, C. B. *J. Chem. Phys.* **1986**, *84*, 788.
(8) Lienau, C.; Williamson, J. C.; Zewail, A. H. *Chem. Phys. Lett.* **1993**, *213*, 289.
(9) Lienau, C.; Zewail, A. H. *Chem. Phys. Lett.* **1994**, *218*, 224.
(10) Lienau, C.; Zewail, A. H. *J. Phys. Chem.* **1996**, *100*, 18629.
(11) Materny, A.; Lienau, C.; Zewail, A. H. *J. Phys. Chem.* **1996**, *100*, 18650.
(12) Wan, C.; Gupta, M.; Baskin, J. S.; Kim, Z. H.; Zewail, A. H. *J. Chem. Phys.* **1997**, *106*, 4353.
(13) Liu, Q.; Wang, J.-K.; Zewail, A. H. *Nature* **1993**, *364*, 427.
(14) Wang, J.-K.; Liu, Q.; Zewail, A. H. *J. Phys. Chem.* **1995**, *99*, 11309.
(15) Liu, Q.; Wang, J.-K.; Zewail, A. H. *J. Phys. Chem.* **1994**, *99*, 11321.
(16) Zadoyan, R.; Li, Z.; Ashjian, P.; Martens, C. C.; Apkarian, V. A. *Chem. Phys. Lett.* **1994**, *218*, 504.
(17) Zadoyan, R.; Li, Z.; Martens, C. C.; Apkarian, V. A. *J. Chem. Phys.* **1994**, *101*, 6648.
(18) Li, Z.; Zadoyan, R.; Apkarian, V. A.; Martens, C. C. *J. Phys. Chem.* **1995**, *99*, 7453.
(19) Zadoyan, R.; Sterling, M.; Ovchinnikov, M.; Apkarian, V. A. *J. Chem. Phys.* **1997**, *107*, 8446.
(20) Chachisvilis, M.; Garcia-Ochoa, I.; Douhal, A.; Zewail, A. H. *Chem. Phys. Lett.* **1998**, *293*, 153.
(21) Zewail, A. H. *J. Phys. Chem.* **1993**, *97*, 12427.
(22) Beeken, P.; Mandich, M.; Flynn, G. *J. Chem. Phys.* **1982**, *76*, 5995.
(23) Beeken, P. B.; Hanson, E. A.; Flynn, G. W. *J. Chem. Phys.* **1983**, *78*, 5892.

(24) Macler, M.; Heaven, M. C. *Chem. Phys.* **1991**, *151*, 219.
(25) Barrow, R. F.; Yee, K. K. *J. Chem. Soc., Faraday Trans. 2* **1973**, *69*, 684.
(26) Tellinghuisen, J. *J. Chem. Phys.* **1973**, *58*, 2821.
(27) Tellinghuisen, J. *J. Chem. Phys.* **1982**, *76*, 4736.
(28) Bergsma, J. P.; Berens, P. H.; Wilson, K. R.; Fredkin, D. R.; Heller, E. J. *J. Phys. Chem.* **1984**, *88*, 612.
(29) Potter, E. D.; Liu, Q.; Zewail, A. H. *Chem. Phys. Lett.* **1992**, *200*, 605.
(30) Fei, S.; Zheng, X.; Heaven, M. C. *J. Chem. Phys.* **1992**, *97*, 6057.
(31) Kelley, D. F.; Abul-Haj, N. A.; Jang, D. J. *J. Chem. Phys.* **1984**, *80*, 4105.
(32) Xu, J.; Schwentner, N.; Chergui, M. *J. Chem. Phys.* **1994**, *101*, 7381.
(33) Batista, V. S.; Coker, D. F. *J. Chem. Phys.* **1996**, *105*, 4033.
(34) Wirnsberger, G.; Fritzer, H. P.; Popitsch, A.; van de Goor, G.; Behrens, P. *Angew. Chem.* **1996**, *108*, 2951.
(35) Wirnsberger, G.; Fritzer, H. P.; Popitsch, A.; van de Goor, G.; Behrens, P. *Angew. Chem., Int. Ed. Engl.* **1996**, *35*, 2777.
(36) Wirnsberger, G.; Fritzer, H. P.; van de Goor, G.; Pillep, B.; Behrens, P.; Popitsch, A. *J. Mol. Struct.* **1997**, *410*−*411*, 123.
(37) Ozin, G. A. *Adv. Mater.* **1992**, *4*, 612.
(38) Behrens, P.; Stucky, G. D. *Comprehensive Supramolecular Chemistry*; Pergamon Press: Oxford, 1996; Vol. 7; p 721.
(39) Meier, W. M.; Olson, D. H.; Baerlocher, C. *Atlas of Zeolite Structure Types*, 4th ed.; Butterworth-Heinemann: London, 1996.
(40) Gies, H. *Z. Kristallogr.* **1986**, *175*, 93.
(41) Wirnsberger, G.; Zink, R.; Pillep, B.; Fritzer, H. P.; Popitsch, A.; Behrens, P. To be published.
(42) Schmitt, M.; Knopp, G.; Materny, A.; Kiefer, W. *Chem. Phys. Lett.* **1997**, *270*, 9.
(43) Knopp, G.; Schmitt, M.; Materny, A.; Kiefer, W. *J. Phys. Chem.* **1997**, *101*, 4852.
(44) Schmitt, M.; Knopp, G.; Materny, A.; Kiefer, W. *J. Phys. Chem. A* **1998**, *102*, 4059.
(45) Rose, T. S.; Rosker, M. J.; Zewail, A. H. *J. Chem. Phys.* **1988**, *88*, 6672.
(46) Mulliken, R. S. *J. Chem. Phys.* **1971**, *55*, 288.
(47) Visnawathan, K. S.; Sur, A.; Tellinghuisen, J. *J. Mol. Spectrosc.* **1981**, *86*, 393.
(48) Tellinghuisen, J. *J. Mol. Spectrosc.* **1982**, *94*, 231.
(49) Tellinghuisen, J. *J. Chem. Phys.* **1985**, *82*, 4012.
(50) Xu, J.; Schwentner, N.; Chergui, M. *J. Chim. Phys.* **1995**, *92*, 541.
(51) Scherer, N. F.; Ziegler, L. D.; Fleming, G. R. *J. Chem. Phys.* **1992**, *96*, 5544.
(52) Paige, M. E.; Harris, C. B. *Chem. Phys.* **1990**, *149*, 37.
(53) Lingle, R., Jr.; Xu, X.; Yu, S.-C.; Zhu, H.; Hopkins, J. B. *J. Chem. Phys.* **1990**, *93*, 5667.
(54) Liu, Q.; Wan, C.; Zewail, A. H. *J. Phys. Chem.* **1996**, *100*, 18666.